

Vortex phase diagram of $\text{Bi}_2\text{Sr}_2\text{CaCu}_2\text{O}_{8+\delta}$: c -axis superconducting correlation in the different vortex phases

M. F. Goffman, J. A. Herbsommer, and F. de la Cruz

Centro Atómico Bariloche, Comisión Nacional de Energía Atómica, S. C. de Bariloche, 8400 RN, Argentina

T. W. Li and P. H. Kes

Kammerling Onnes Laboratory, Rijksuniversiteit Leiden, P.O. Box 9506 2300 RA Leiden, The Netherlands

(Received 8 August 1997)

The vortex phase diagram in $\text{Bi}_2\text{Sr}_2\text{CaCu}_2\text{O}_{8+\delta}$ is investigated by studying the linear ac transverse permeability $\mu_{\perp} = \mu'_{\perp} + \mu''_{\perp}$ ($h_{ac} \perp H \parallel c$ axis) in a wide range of temperature and magnetic fields. At low fields ($H < 300$ Oe) superconducting phase coherence in the c direction shows that the ordered vortex solid state is characterized by a c -axis vortex correlation length l_c limited by the sample thickness d . At low temperatures ($T < 20$ K) point disorder is sufficiently strong and the phase coherent ordered vortex solid becomes metastable. In the temperature range $20 < T < 42$ K when the applied field exceeds $H_{ent}(T)$, the ordered vortex state transforms into an entangled state with no indication of reduction of l_c . At a higher crossover field the linear response becomes Ohmic, $l_c < d$. At higher temperatures the vortex structure becomes an uncorrelated vortex liquid in all directions. [S0163-1829(98)02706-4]

The superconducting H - T phase diagram of $\text{Bi}_2\text{Sr}_2\text{CaCu}_2\text{O}_{8+\delta}$ (BSCCO) is the paramount example of high-temperature oxide superconductors showing the relevant characteristics associated with the properties of the layered compounds: strong anisotropy, thermal fluctuations, and atomic disorder.

In Fig. 1 we plot a sketch of the H - T phase diagram of BSCCO including those lines that are broadly accepted as dividing regions of the phase diagram with different static and/or dynamic properties of the corresponding vortex structures. Despite this, there is no consensus on which of them corresponds to true thermodynamic phase transitions or to a crossover from one characteristic dynamic response to another dynamic regime. More importantly, the nature of the vortex structures it is not fully known in the different regions of the phase diagram. One exception is the line indicated by $T_M(H)$ corresponding to the first order phase transition^{1,2} from an ordered vortex solid at low temperatures to a liquid phase at higher temperatures. However, although the transport measurements show³ Ohmic behavior in the liquid state in both directions (ρ_c and ρ_{ab} different from zero) there is no conclusive experimental evidence demonstrating whether the liquid is made of vortex lines cutting and reconnecting at an average distance l_c , defining the superconducting phase correlation length in the c direction or of decoupled vortex pancakes, l_c equals the interplane distance s . From previous discussions and from transport experiments using multiterminal contact configuration in YBCO it has also become evident⁴ the important role that l_c plays in determining the properties of the vortex structure in the different regions of the phase diagram.

In this work we analyze the different suggestions found in the literature on the nature of the vortex structure in the different regions of the phase diagram in Fig. 1 in terms of what should be expected for the superconducting response in the c direction and the related vortex correlation length l_c . It

is important to point out that most of the experiments made in BSCCO concentrate their study on the properties associated with the current response in the ab direction and little attention has been devoted to the response in the c direction.

The results reported in this paper are obtained measuring the transverse ac permeability μ_{\perp} in the linear regime. The dc magnetic field H is applied parallel to the c direction and a small ac field h_{ac} is induced perpendicular to H . In this way the ac currents induced in the sample are forced to flow in both directions, on the ab planes and across the sample thickness. The real component μ'_{\perp} is related to the shielding capability of the currents while μ''_{\perp} , the imaginary part, is straightforwardly related to the dissipation induced by the ac

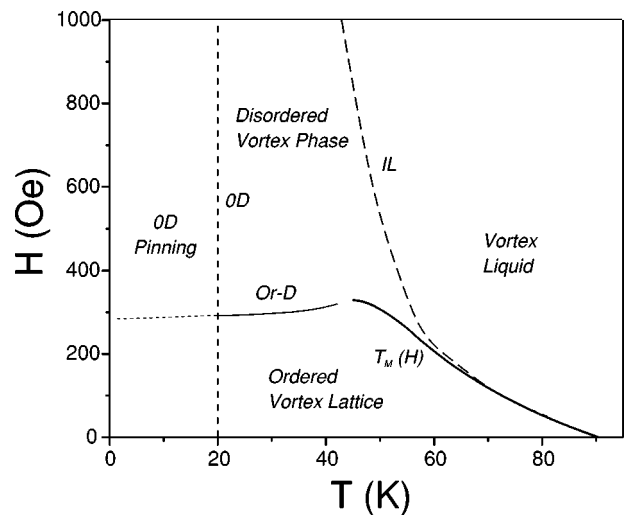


FIG. 1. Schematic phase diagram of BSCCO indicating the position and shape of the irreversibility line (IL), the melting line $T_M(H)$, and the Or-D line discussed in the text. The dashed line OD represents the boundary of a zero-dimensional pinning regime (pancake vortices individually pinned) at low temperatures.

currents. The amplitude and frequency dependence of μ_{\perp} and the relation between μ'_{\perp} and μ''_{\perp} determine⁵ the linear and/or Ohmic characteristics of the response. This technique has proved¹ to be adequate to study BSCCO in regions of the phase diagram where the low value of the resistivity and the aspect ratio of the samples make the conventional dc transport measurements useless.

We show that the transverse permeability μ_{\perp} at low fields is consistent with a highly correlated (topologically ordered) vortex solid state which is superconducting in all directions. At a higher field $H_{\text{em}}(T)$ and for $T > 20$ K the long-range vortex correlation in the c direction is retained at the topological order-disorder transition of the vortex structure up to a crossover field $H_{\text{cr}}(T)$ where the response in the c direction becomes Ohmic, indicating that the structure loses its superconducting character. By all experimental indications, the vortex ensemble below 20 K is a nonequilibrium superconducting vortex solid structure.

The line IL in Fig. 1 is the irreversibility line, typically determined by the onset of hysteresis in the magnetization curve associated with currents flowing in the ab planes and $T_M(H)$ is the first order melting line of the vortex structure. In the low field range IL is known⁶ to be determined by geometrical barriers (GB's). The longitudinal ac permeability ($h_{\text{ac}} \parallel H$) in the linear regime shows an Ohmic behavior with the corresponding peak in μ''_{\parallel} at temperatures close but always *above* either $T_M(H)$ or the IL line,⁷ depending on the range of fields, indicating that the Ohmic resistance in the ab planes become undetectable below those lines.

Pastoriza *et al.*¹ have pointed out that μ'_{\perp} shows a frequency-independent peak associated with the establishment of the phase coherence across the sample at the melting temperature. That is, for $T < T_M(H)$ l_c is limited by the sample thickness d as is expected in a topologically ordered structure of vortex lines. The same type of measurements (for low enough frequencies) demonstrated⁸ that at higher fields the dissipation in the c direction was Ohmic and finite well below IL. No superconductivity is established at IL in the c direction and, consequently, $l_c < d$ in a region where the resistance in the ab planes is either zero or below the detectable values.

There is⁹⁻¹¹ a phase boundary or crossover separating two solid regions in the phase diagram, indicated by Or-D in Fig. 1. This line is essentially field independent and takes place at a field of the order of 300 Oe. The observation of an anomalous sharp second peak in the magnetization loop has been used to define the Or-D boundary. Moreover, no data is reported in the literature showing the presence of the second peak below 20 K. The Or-D line has been interpreted as a crossover in the pinning mechanism,⁹ as a change in the dynamic properties of the vortex lattice,¹⁰ or as a true phase transition.¹¹ Neutron diffraction¹² and muon spin rotation experiments¹³ show that the vortex structure changes from an ordered one for fields below Or-D to a topologically disordered structure in the higher field region. Moreover, the results of Ref. 1 indicate that l_c changes from $l_c = d$ in the ordered low-field region to $l_c < d$ at high fields. From the previous discussion it is interesting to determine whether the Or-D line marks also the evolution from the Ohmic behavior in the c direction for high fields to a superconducting regime at low fields.

Recent flux relaxation experiments¹⁰ below 20 K and at low fields have been interpreted assuming that the elastic Larkin length L_c equals s , the Cu-O interplane distance. This means that the pinning mechanism is described in the zero-dimensional limit, where every pancake is pinned independently of the others. At this temperature the transverse susceptibility decreases rapidly⁷ indicating that perfect screening is established. In this limit l_c is limited by the sample thickness $l_c = d$ and $L_c = s$. According to Ref. 10 a vertical line (indicated as 0D in Fig. 1) at 20 K indicates the zero-dimensional pinning limit that takes place at low temperatures. Thus, the pinning line should intersect with the Or-D line and consequently it is interesting to ask whether the order-disorder transition (Or-D) remains below 20 K and which is the corresponding correlation length l_c . As we will show in this paper the measurement of the transverse permeability is a unique technique to explore the solid state phases and determine its superconducting characteristics in the c direction.

The BSCCO crystals were grown by the traveling solvent floating zone technique.¹⁴ The experiments were performed on two crystals (A and B) with dimensions $3000 \times 2000 \times 180 \mu\text{m}^3$ and $3000 \times 2000 \times 70 \mu\text{m}^3$, respectively. After annealing in air at 800 °C the critical temperature of these optimally doped crystals is $T_c = 90.5$ K. The ac susceptibility measurements were carried out by means of two complementary techniques. For measurements at frequencies higher than 500 Hz a conventional mutual inductance technique was used. For low frequencies ($10^{-2} - 10^3$ Hz) the measurements were carried out using a superconducting quantum interference device (SQUID) as a preamplifier. The ac field was applied parallel to the ab planes of the sample by means of a Helmholtz solenoid. The excitation current that feed the Helmholtz solenoid was taken from the reference signal of a two phase lock-in amplifier (PAR 5302). The pick-up coil is made of Nb wire wound in a transverse first order gradiometer configuration. This coil is part of the superconducting transformer of the SQUID. The change of the sample permeability as a function of field and temperature induces a current in the pick-up coil which is detected by the SQUID. The in and out of phase components of this current were measured by the lock-in amplifier connected at the output of the SQUID electronics. The proper phase of the lock-in amplifier was set by measuring the sharp superconducting transition of an indium sample. The dc field was applied parallel to the c axis of the sample by means of a home-made superconducting magnet operated in a permanent mode. Further experimental details can be found in Ref. 7. All the ac permeability measurements reported here have been taken in field cooling (FC) experiments.

The ac permeability data presented were taken at an ac field amplitude $h_{\text{ac}} \leq 90$ mOe. The response for this ac amplitude was proved to be within the linear regime in the whole range of dc fields and temperatures investigated.

Shown in Fig. 2 are typical data of the real part of the ac permeability μ'_{\perp} as a function of temperature for four selected frequencies at a field of 27 Oe. The main feature observed at high temperatures is the sharp decrease of μ'_{\perp} , at a frequency-independent temperature $T_M(H)$ reported in Ref. 1 that we will not discuss here. Lowering the temperature μ'_{\perp}

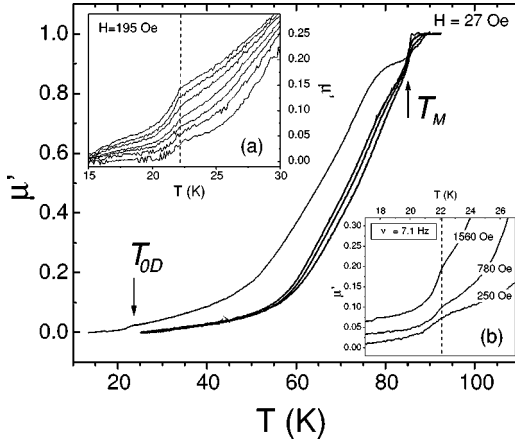


FIG. 2. Real part of the ac permeability μ'_{\perp} as a function of temperature for four selected frequencies. From left to right: 7.1, 2300, 6525, and 18 300 Hz. Inset (a) shows an expanded view of the low-temperature region for different excitation frequencies. From left to right: 0.5, 1.16, 2.30, 7.12, 17.6, 38.9, 108.3 Hz. The sudden decrease in μ'_{\perp} is seen at a frequency-independent temperature T_{0D} . Inset (b) shows μ'_{\perp} for three selected fields. T_{0D} is field independent in the range of fields investigated (20–1600 Oe).

decreases smoothly and a second feature at $T_{0D} \approx 22$ K becomes evident⁷ in the low-frequency curve. The inset (a) clearly shows that the temperature T_{0D} , where a steep decrease in μ'_{\perp} takes place, is frequency independent. It is also shown that this drop at T_{0D} is smeared out and becomes undetectable when increasing the excitation frequency to the range of kHz. In inset (b) we depicted the data of $\mu'_{\perp}(T)$ at three selected dc fields. This exemplifies that T_{0D} is field independent in the range of fields investigated (20–1600 Oe).

The low-field response as detected by $\mu_{\perp}(T)$ can be understood in the following way. Below the melting temperature $T_M(H)$ the ac field generates a surface shielding current which exerts a tilting stress on the vortex lattice (VL). The resulting deformation of the VL at the surface propagates into the interior, pushed forward by the elastic response of the VL and slowed down by point quenched disorder and viscous drag. The ac complex penetration depth $\lambda_{ac}(\omega)$, considering the mechanisms described above is^{15,16}

$$\lambda_{ac}^2(\omega) = \frac{\lambda^2 + \lambda_c^2 [\alpha_L(\omega)/\alpha_L + i\omega\tau_d]^{-1}}{1 + i\omega\tau_{nf}}, \quad (1)$$

where ω is the excitation frequency, λ^2 and $\lambda_c^2 = C_{44}(\mathbf{k})/\alpha_L$ denote the London and the Campbell penetration depths, respectively, and $\tau_d = \eta/\alpha_L$ and $\tau_{nf} = \lambda^2 \mu_o / \rho_n$ the damping times associated with the oscillation, characterized by the viscous drag coefficient η and the normal resistivity ρ_n . $C_{44}(\mathbf{k})$ is the dispersive tilt modulus of the VL and $\alpha_L(\omega)$ the linear restoring force per unit volume of an elastically pinned VL (Labusch parameter). The frequency dependence of the Labusch parameter $[\alpha_L(\omega)/\alpha_L]$ takes into account the flux creep present in the whole range of temperatures.¹⁷

In this low-frequency range μ_{\perp} is almost real (the imaginary part is always below 0.03), therefore the complex ac penetration depth λ_{ac} related to the ac permeability via μ_{\perp}

$= (\lambda_{ac}/d) \cdot \tanh(d/\lambda_{ac})$ is approximately equal to the Campbell penetration depth, determined by

$$\lambda_{ac}^2 \approx \frac{C_{44}(\mathbf{k})}{\alpha_L(\omega)}. \quad (2)$$

In Eq. (2) the superfluid contribution was also neglected. At high temperatures the critical current in BSCCO crystals is small, indicating that the Larkin domains are large and the VL is pinned collectively. When the temperature is lowered the pinning becomes more efficient, the elastically correlated volume (Larkin domains) shrinks, the Labusch parameter increases, and consequently the penetration of the tilting stress λ_{ac} decreases. The steep decrease of μ'_{\perp} at $T \approx 22$ K indicating almost perfect shielding coincides with the large increase in the critical current inferred from magnetization measurements,¹⁸ associated with the crossover to the zero-dimensional pinning regime. It is important to point out that although the BSCCO crystals studied present the first order phase transition at high temperatures, characteristic of *clean* systems, strong disorder sets in at temperatures below 22 K, where the steep decrease of μ'_{\perp} coincides with the crossover to a region where the pinning mechanism is 0D,¹⁹ that is, $L_c \approx s$.

We turn now to the question of the nature of the second peak transition and its relation with l_c . Since this transition or crossover is observed at an almost temperature-independent field we study the ac permeability at fixed temperature as a function of the dc applied field. The results are shown in Fig. 3. We remark that $\mu_{\perp}(T)$ was measured decreasing temperature at constant field (FC experiment) for different dc applied fields and then the field dependence at fixed temperature $\mu_{\perp}(H)$ was obtained from these measurements. In this way effects associated with gradients of fields inside the sample, present when measuring magnetization loops or flux relaxation, are minimized. The results displayed in Fig. 3(a) correspond to a frequency of 6525 Hz, while the data presented in Fig. 3(b) corresponds to an excitation frequency of 4.5 Hz, approximately three orders of magnitude lower. We distinguish three qualitatively different behaviors.

(i) At temperatures $T \leq 20$ K, where the disorder is strong, μ'_{\perp} increases monotonically with increasing field. This is expected, since the tilt modulus C_{44} is an increasing function of the magnetic field.

(ii) In the intermediate regime of temperatures $20 \leq T \leq 42$ K, μ'_{\perp} is an increasing function of H up to the dc field $H_{ent}(T)$. For $H > H_{ent}(T)$, μ'_{\perp} decreases until the field $H_{cr}(T)$ is reached, where μ'_{\perp} starts to increase abruptly. The unusual behavior (the decrease of μ'_{\perp} when increasing the dc field) that begins at $H_{ent}(T)$ marks the improvement of the effectiveness of pinning when increasing field. This can be interpreted as an evidence of the proliferation of topological defects at large scale in the ordered VL.²⁰ This proliferation generates vortex entanglement²¹ and, provided that the line crossing barriers are large, would increase the effectiveness of pinning, similar to the ideas proposed by Hwa *et al.*²² with regard to enhanced pinning by splay columnar defects. With further increases in magnetic field, the topological defects become denser bringing larger vortex crossing angles, flux cutting becomes easier, and the effectiveness of pinning drops. The abrupt increase in μ'_{\perp} from $H_{cr}(T)$ indicates the

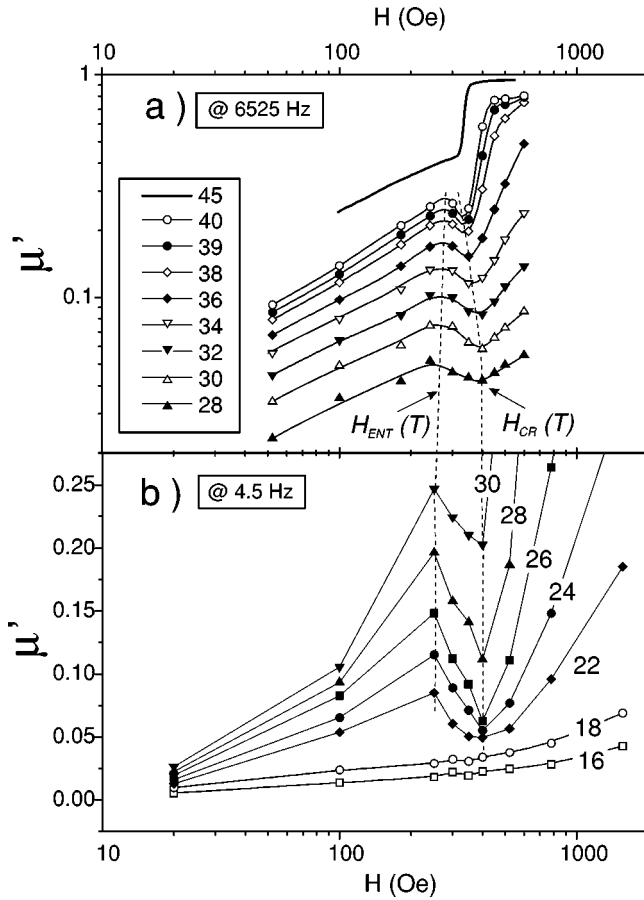


FIG. 3. Real part of the ac permeability μ'_\perp as a function of field. The numbers indicate the temperature in K. Part (a) of the figure shows the results obtained at a high frequency (6525 Hz) and part (b) at a low frequency (4.5 Hz). The dashed lines indicate the characteristic fields $H_{\text{ent}}(T)$ and $H_{\text{cr}}(T)$ (see text). The nonmonotonic behavior in μ'_\perp is not observed for temperatures below 20 K.

evolution towards the c -axis Ohmic state at higher fields,⁷ that is, towards a state where the phase coherence is lost across the sample. The nonmonotonic behavior observed in this temperature regime is detected at low and high excitation frequencies, and $H_{\text{ent}}(T)$ and $H_{\text{cr}}(T)$ are found to be frequency independent. This fact discards the interpretation of $H_{\text{ent}}(T)$ as a dynamic effect due to a change in the pinning mechanism.²³

(iii) In the high-temperature regime $T \geq 45$ K, μ'_\perp increases smoothly up to $H_M(T)$, where a jump to $\mu'_\perp \approx 1$ is observed. This jump is associated with the first order phase transition of the vortex lattice, as was previously reported.¹

Our results could be summarized in the experimental H - T phase diagram depicted in Fig. 4. At low temperatures ($T < 20$ K) point disorder is sufficiently strong to induced zero-dimensional pinning, $L_c \approx s$, and strong critical currents in the ab planes. In principle, $L_c \approx s$ would imply a highly disordered vortex structure, in contradiction with the results found in neutron diffraction experiments¹² where a crystalline structure is detected at temperatures well below 20 K. Both experimental results can be reconciled considering that the structure detected below 20 K is frozen at a higher temperature where the vortex-vortex interaction is dominant, similar to the recent interpretation by Pardo *et al.*²⁵ of mag-

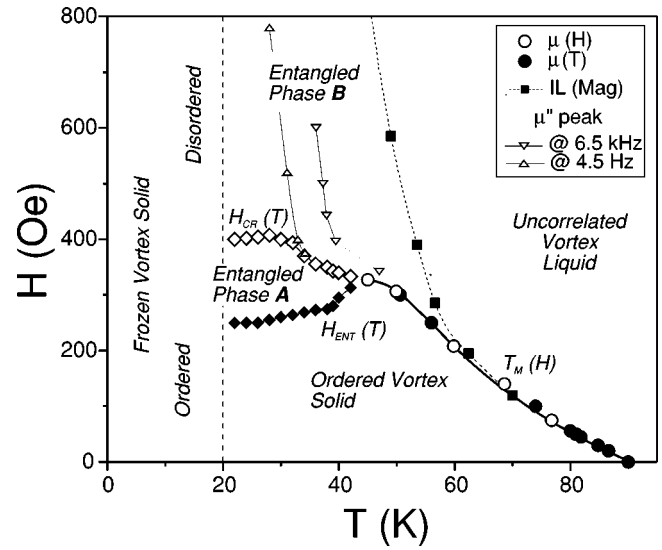


FIG. 4. Experimental phase diagram of BSCCO. Open circles correspond to $T_M(H)$ determined by $\mu(H)$ measurements while filled circles correspond to $T_M(H)$ determined by $\mu(T)$ measurements. Closed squares correspond to the IL line determined by ZFC-FC magnetization measurements. Solid and open diamonds represent the characteristics fields $H_{\text{ent}}(T)$ and $H_{\text{cr}}(T)$, respectively. Open triangles: peak position in μ'_\perp for 4.5 Hz and 6525 Hz. Thin lines represent c -axis constant resistance contours. The ordered VL solid stable at low fields transforms upon raising the field above $H_{\text{ent}}(T)$ to an entangled phase A and becomes an uncorrelated liquid increasing the temperature above $T_M(H)$. The disordered solid A evolves towards a phase B characterized by an Ohmic response in the c -axis direction. Below 20 K the solid is frozen in a state that depends on the experimental history.

netic decoration experiments showing the presence of topologically ordered vortex structures in the low-field range where the critical current is field independent and vortices are individually pinned. The vortex structure is frozen in a topological configuration corresponding to a higher temperature where the lattice is nearly in thermodynamic equilibrium. Further decrease of temperature only induces small local displacements of the vortex, in distances of the order of the pinning force range ξ , much smaller than the intervortex separation and the overall vortex structure remains unmodified. Under these circumstances it is clear that while the critical current is independent of the geometrical vortex distribution, the vortex structure depends on the experimental history. As a consequence the observation of Bragg peaks in the low-temperature and low-field phases only reflects a non-equilibrium vortex configuration corresponding to a stable structure at higher temperatures.

In the intermediate regime ($20 \leq T \leq 42$ K) the ordered vortex solid become unstable at a field $H_{\text{ent}}(T)$, where the effectiveness of pinning starts to increase with increasing field as indicates the drop of μ'_\perp . The functional dependence of $H_{\text{ent}}(T)$ is in good qualitative agreement with theoretical estimates.²¹ Furthermore, we evaluate the field at which the ordered vortex state become unstable at low temperatures using the expression (11) of Ref. 24:

$$H_{\text{ent}} \approx \frac{(\pi c_L)^4}{(16\pi)^{1/3} \pi^2} \left(\frac{\epsilon_0}{U_p} \right)^{4/3} H_{c2}^{2/3} H_{\text{cross}}^{1/3}, \quad (3)$$

where we have introduced the crossover field $H_{\text{cross}} \approx \pi \ln(\gamma d/\xi) \Phi_0 / (\gamma s)^2$ (Ref. 26), γ is the anisotropy parameter, $H_{c2} = \Phi_0 / 2\pi \xi^2$, $\varepsilon_0 = (\Phi_0 / 4\pi \lambda)^2$, and c_L the Lindemann constant usually of the order of $c_L \sim 0.1 - 0.2$. The anisotropy parameter $\gamma = 110$ is extracted from the fitting of $T_M(H)$ at high temperatures using the decoupling expression of Refs. 11,26,27. Using the previous reasonable values for optimally doped BSCCO crystals, $H_{\text{cross}} \approx 10\,900$ Oe, $H_{c2} \approx 8.2 \cdot 10^5$ Oe, $U_p/\varepsilon_0 \approx 0.085$, and $c_L = 0.1$ gives $H_{\text{ent}} \approx 250$ Oe in fair agreement with the observed experimental value.

At the field $H_{\text{ent}}(T)$ the ordered VL makes the transition to a vortex entangled state with no indication of a reduction in l_c . When increasing the field the energy barrier for vortex cutting and reconnection decreases and $H_{\text{cr}}(T)$ marks a crossover to an Ohmic behavior characterized by $l_c < d$. At higher temperatures ($T > 45$ K) the ordered vortex phase transforms to an uncorrelated vortex liquid in all directions through the well-known first order phase transition.

In conclusion we show that the ac permeability technique is an excellent tool to explore the vortex matter phase diagram of highly layered superconductors. It allows us to probe the tilting strength and to establish the correlation in the c -axis direction of the different regions of the phase diagram. The data taken in FC experiments allows us to study the vortex structure minimizing forces induced on the vortex ensemble by nonequilibrium currents associated with field gradients.

The large ac penetration of the transverse field in the ordered solid at high temperatures is consistent with the idea that this state is close to thermodynamic equilibrium and provides strong support to the picture where the field-induced transition at the Or-D line is a thermodynamic transition. The data has shown that the Or-D transition has strong influence on the behavior of the vortex correlation in the

field direction. Vortex tilting is harder for fields above $H_{\text{ent}}(T)$ showing that the Or-D transition, induced by point defects, is from a three-dimensional ordered structure to an entangled phase of correlated vortex lines across the sample (entangled phase A in Fig. 4). The vortex phase correlation in the c direction is preserved at the transition. At higher fields flux cutting and reconnection is dominant, the ac transverse field penetrates easily, and the response becomes ohmic at fields above the crossover field $H_{\text{cr}}(T)$, where $l_c < d$. In the low-temperature region of the phase diagram ($T < 20$ K) and for all the fields investigated, the pinning is strong enough to freeze the vortex structure in an experimental history-dependent state. The zero-dimensional pinning limit associated with this region of the phase diagram is consistent with results that could be considered contradictory: At low fields the neutron diffraction experiments¹² shows the FC structure frozen in an ordered state. For fields higher than 400 Oe the structure is found to be disordered. Neither the critical currents nor perpendicular permeability measurements detect any change that could be associated with an order-disorder transition of the vortex ensemble at low temperatures. This is understood realizing that neutron diffraction experiments provide information about the topological order of the vortex structure over large regions compared to the average intervortex distance. Meanwhile, the critical current and perpendicular permeability measurements, in the individual pinning regime, respond mainly to the local pinning of a single vortex independently of the space correlation of the vortex structure.

We thank H. Pastoriza for fruitful discussions and E. F. Righi for a critical reading of the manuscript. This work was partially support by Fundacion Antorchas (Grant No. A-13359/1-000013) and the Consejo Nacional de Investigaciones Científicas y Técnicas (CONICET) (Grant No. CO 21418/95).

- ¹H. Pastoriza, M. F. Goffman, A. Arribére, and F. de la Cruz, Phys. Rev. Lett. **72**, 2951 (1994).
- ²E. Zeldov *et al.*, Nature (London) **375**, 373 (1995).
- ³D. T. Fuchs *et al.*, Phys. Rev. B **55**, 6156 (1997).
- ⁴D. Lopez, E. F. Righi, G. N. Nieva, and F. de la Cruz, Phys. Rev. Lett. **76**, 4034 (1996).
- ⁵See, for example, X. Ling and J. Budnick, in *Magnetic Susceptibility of Superconductors and Other Spin Systems*, edited by R. A. Hein, T. L. Francavilla, and D. H. Liebenberg (Plenum, New York, 1991), p. 337, and references therein.
- ⁶E. Zeldov *et al.*, Phys. Rev. Lett. **73**, 1428 (1994).
- ⁷A. Arribére, H. Pastoriza, M. F. Goffman, F. de la Cruz, D. B. Mitzi, and A. Kapitulnik, Phys. Rev. B **48**, 7486 (1993).
- ⁸F. de la Cruz *et al.*, Physica B **197**, 596 (1994).
- ⁹T. Tamegai, Y. Iye, I. Oguro, and K. Kishio, Physica C **213**, 33 (1993).
- ¹⁰M. Nideröst *et al.*, Phys. Rev. B **53**, 9286 (1996).
- ¹¹B. Khaykovich *et al.*, Phys. Rev. Lett. **76**, 2555 (1996).
- ¹²R. Cubitt *et al.*, Nature (London) **365**, 407 (1993).
- ¹³S. L. Lee *et al.*, Phys. Rev. Lett. **71**, 3862 (1993).
- ¹⁴T. W. Li *et al.*, J. Cryst. Growth **135**, 481 (1993).
- ¹⁵M. Coffey and J. Clem, Phys. Rev. B **45**, 10 527 (1992).
- ¹⁶E. H. Brandt, Physica C **195**, 1 (1992).
- ¹⁷The frequency dependence could be evaluated using the Brandt's

linear response ansatz Eq. (26) of Ref. 16 and it is a subject of current investigation.

- ¹⁸C. J. van der Beek *et al.*, Physica C **195**, 307 (1992).
- ¹⁹G. Blatter *et al.*, Rev. Mod. Phys. **66**, 1125 (1994).
- ²⁰E. H. Brandt, Phys. Rev. B **34**, 6514 (1986); R. Wördenweber and P. H. Kes, *ibid.* **34**, 494 (1986).
- ²¹D. Ertas and D. R. Nelson, Physica C **272**, 79 (1996); M. J. P. Gingras and D. A. Huse, Phys. Rev. B **53**, 15 193 (1996); J. Kierfeld, T. Nattermann, and T. Hwa, *ibid.* **55**, 626 (1997); D. Carpentier, P. Le Doussal, and T. Giamarchi, Europhys. Lett. **35**, 379 (1996); D. S. Fisher, Phys. Rev. Lett. **78**, 1964 (1997).
- ²²T. Hwa *et al.*, Phys. Rev. Lett. **71**, 3545 (1993).
- ²³The frequency of the ac excitation fixes the *time scale* of the experiment, therefore at high frequencies ($\sim 10^4$ Hz) the time scale is very short ($t \sim 10^{-4}$ sec) and one would expect (since the effects of creep would be negligible) a decrease of the effectiveness of pinning as soon as the pinning mechanism changes from individual to collective increasing the magnetic field, instead of what is observed in our transverse permeability measurements.
- ²⁴T. Giamarchi and P. Le Doussal, Phys. Rev. B **55**, 6577 (1997).
- ²⁵F. Pardo *et al.*, Phys. Rev. B **55**, 14 610 (1997).
- ²⁶L. I. Glazman and A. E. Koshelev, Phys. Rev. B **43**, 2835 (1991).
- ²⁷L. L. Daemen, L. N. Bulaevskii, M. P. Maley, and J. Y. Coulter, Phys. Rev. B **47**, 11 291 (1993).